Available online at www.sciencedirect.com
SCIENCE DIRECT®
Journal of Nuclear Materials 340 (2005) 219–236
journal of nuclear materials
www.elsevier.com/locate/jnucmat

Mechanism of irradiation assisted stress corrosion crack initiation in thermally sensitized 304 stainless steel

T. Onchi [a,*], K. Dohi [a], N. Soneda [a], Marta Navas [b], M.L. Castaño [b]

[a] Central Research Institute of Electric Power Industry (CRIEPI), 2-11-1, Iwado Kita, Komae-shi, Tokyo 201-8511, Japan
[b] CIEMAT. Avda. Complutense, 22, 28040 Madrid, Spain

Received 24 February 2004; accepted 26 November 2004

Abstract

Thermally sensitized 304 stainless steels, irradiated up to 1.2×10^{21} n/cm^2 ($E > 1$ MeV), were slow-strain-rate-tensile tested in 290 °C water containing 0.2 ppm dissolved oxygen (DO), followed by scanning and transmission electron microscopic examinations, to study mechanism of irradiation-assisted-stress-corrosion-crack (IASCC) initiation. Intergranular (IG) cracking behaviors changed at a border fluence (around 1×10^{20} n/cm^2), above which deformation twinning were predominant and deformation localization occurred earlier with increasing fluence. The crack initiation sites tended to link to the deformation bands, indicating that the crack initiation may be brought about by the deformation bands interacted with grain boundaries. Thus the border fluence is equivalent to the IASCC threshold fluence for the sensitized material, although the terminology of IASCC is originally given to the non-sensitized materials without microstructural definition. The IASCC threshold fluence was found to change with irradiation conditions. Changes in IASCC susceptibility and IASCC threshold fluence with fluence and DO were further discussed.

PACS: 61.72.Lk; 61.72.Mm; 61.72.Nn; 61.80.HG; 61.82.Bg; 62.20.Fe; 68.37.Hk; 68.37.Lp

1. Introduction

Austenitic stainless steels (SSs) used for the light water reactor components tend to suffer from degradation in the environment of radiation and high temperature water during long-term service. Two kinds of material degradation phenomena, namely, irradiation assisted stress corrosion cracking (IASCC) and intergranular stress corrosion cracking (IGSCC) for the irradiated, non-sensitized SSs and the non-irradiated, thermally sensitized SSs, respectively in water environment are known, although their behaviors are similar to each other. Their primary cause has been attributed to the grain boundary chromium (Cr) depletion, produced either by welding during fabrication for IGSCC [1], or by radiation induced segregation (RIS) during service for IASCC [2]. The Cr depletion theory however is nowadays uncertain due to the facts that austenitic 304L and/or 316L SSs having no grain boundary Cr depletion are unable to prevent IGSCC in the BWR water environment [3]. Although premature failure by intergranular environmental cracking of materials exposed to ionizing irradiation has originally termed as IASCC [2] and many metallurgical

* Corresponding author. Tel.: +81 3 3480 2111; fax: +81 3 3489 0700/3480 7950.
E-mail address: tonchi@criepi.denken.or.jp (T. Onchi).

0022-3115/$ - see front matter © 2005 Elsevier B.V. All rights reserved.
doi:10.1016/j.jnucmat.2004.11.012

factors such as radiation hardening, ductility loss, RIS of alloying elements of Cr and Ni and residual elements at grain boundaries and radiation induced microstructural evolutions appear to be influential, it is essential for mechanistic understanding of IASCC to identify what the mechanism of intergranular (IG) crack initiation, and how metallurgical factors noted above affect IG crack initiation. In this regards, a recent work of Busby et al. [4] on post-irradiation annealing of proton-irradiated austenitic SSs showed that the IG cracking susceptibility in BWR water changed while leaving RIS virtually unchanged, indicating that Cr depletion is not the primary determinator for IASCC. On the contrary Fukuya et al. [5] more recently insisted that grain boundary segregation, probably Cr depletion, was sufficient to cause IASCC in oxygenated water, based on microstructural observation, grain boundary compositional analyses and slow strain rate tensile (SSRT) tests in 561K oxygenated water for solution annealed SUS 304L, 316 and 316LSSs irradiated to 0.8 dpa in a material test reactor. The above two works apparently suggests that the role of Cr depletion on the mechanistic process of IASCC has not decisively been proved.

Presence of neutron fluence threshold for IASCC at about 5×10^{20} n/cm^2, corresponding to about 0.7 dpa, for the solution annealed austenitic SSs in BWR condition has been a consensus in the IASCC study community [6]. This threshold fluence has been determined phenomenologically from post-irradiation laboratory tests that exhibit a characteristic rise in susceptibility, in addition to from field experiences, without considering mechanistic IG crack initiation process of the irradiated austenitic stainless steels. It is unsuccessful to ascribe the presence of the threshold fluence for IASCC to the RIS-induced chromium depletion. It is still uncertain what the IASCC threshold fluence actually implies, and what the mechanistic process of IASCC initiation is. Therefore the objective of this work is to identify mechanistic meanings of the fluence threshold for IASCC by examining tensile properties, IG cracking responses, fractographic and microstructural features as a function of neutron fluence. Attention is focused on mechanical aspects of IG crack initiation in oxygenated water, since it has been proved that IG cracking can occur without involvement of water environment on the surface region of the irradiated, thermally sensitized 304 SS [7,8]. The presence of mechanism mechanically causing IG cracking in inert gas in the irradiated, thermally sensitized 304 SS suggests that even if IG cracking occurs during SSRT tests in water environment, water itself is not absolutely effective for nucleating and initiating IG cracks. Based on mechanistic consideration of IG crack initiation process in inert gas, we hypothesize that high stress and strain concentrations at grain boundaries are more essential than the water environment for IG crack initiation [8].

2. Experimental

The tensile specimens were fabricated from a solution annealed 304 SS tube having an outer diameter of 10 mm and a thickness of 1 mm. The shape and dimension of the specimen are shown in Fig. 1. The gauge section of the tensile specimen is 16 mm long and 3 mm wide, and one side of the specimen is convex and the other concave. The chemical composition of the unirradiated 304 SSs sample is shown in Table 1. The solution annealed 304 SS specimens were further heat-treated in two steps: at 750 °C for 100 min and then at 500 °C for 24 h. These heat treatments produced thermally sensitized microstructures, that is, a large variety of chromium carbide precipitate at grain boundaries in the 304 SSs, resulting in large changes in chemical compositions, especially Cr depletion at the grain boundary. The concentrations of major alloying elements at grain boundaries of the thermally sensitized material, measured by field emission typed transmission electron microscopy, were Cr: 11.0, Ni: 12.0 and Fe: 75.2 wt%.

The thermally sensitized 304 SS tensile specimens were irradiated to neutron fluences ranging from 7.5×10^{19} to 1.2×10^{21} n/cm^2 ($E > 1$ MeV) in test reactors. Table 2 summarizes the irradiation conditions of the specimen. All the specimens were irradiated in the capsules filled with helium gas, except for those of the highest fluence, which were irradiated in an environment of oxygenated pure water. Neutron irradiation in water apparently formed thicker specimen surface oxides films than that in inert gas did. There is however no clear evidence for the irradiation environment of oxygenated water to have affected the occurrences of IG cracking in this work. It has been demonstrated that neutron irradiation to around 10^{21} n/cm^2 causes a reduction in grain boundary chromium concentration by only a few % for the thermally sensitized 304 SS [9].

A SSRT technique was applied for the tensile tests of the unirradiated and irradiated specimens at 290 °C in inert gas and in oxygenated water containing 0.2 ppm dissolved oxygen (DO) at the CIEMAT hot cell facility.

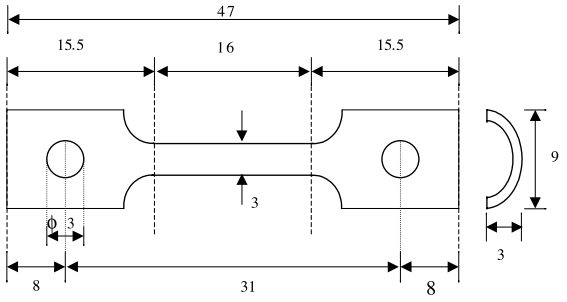

Fig. 1. Shape and dimension of the tensile specimen.

Table 1
Chemical composition of the unirradiated, thermally sensitized 304 SS (wt%)

Chemical elements	C	Si	Mn	P	S	Ni	Cr	Co	Fe
304 SS	0.05	0.61	0.88	0.022	0.014	9.4	18.6	0.002	Bal.

Table 2
Irradiation conditions of the tensile specimen

Neutron fluence (n/cm^2, $E > 1$ MeV)	Irradiation temperature (°C)	Irradiation environment	Neutron flux (n/cm^2/s, $E > 1$ MeV)	Irradiation reactor
7.5×10^{19}	190	Helium gas	5×10^{13}	JMTR
1.1×10^{20}	185	Helium gas	5×10^{13}	JMTR
6.2×10^{20}	290	Helium gas	2×10^{13}	Halden reactor
1.2×10^{21}	290	Pure water	4×10^{13}	Halden reactor

An average strain rate of 3.5×10^{-7} s^{-1} (a cross head speed of 0.33 μm/min) was used. The DO concentration was maintained during the tests though no measurements of corrosion potential were made. The water conductivity at the inlet and outlet of the test section was less than 0.1 μS/cm. Mechanical properties of the unirradiated and irradiated specimens were determined from the chart recording during the SSRT in inert gas.

Scanning electron microscopy (SEM) was used to examine detailed fractographic aspects of all the fractured specimens. Prior to the SEM, the fractured specimens were ultrasonically cleaned. Some specimens fractured in 0.2 ppmDO water were further electrically cleaned in a solution of 12 wt%NaCN and 5.7 mol/lNaOH to remove corrosion product deposits on the fracture surface and the specimen surface.

Transmission electron microscopy (TEM) observations of the fractured specimens were made at the BNFL hot facility. The TEM foils were prepared from the gauge length to obtain slices parallel to fracture face. A slice for the TEM was taken from the un-necked portion away from the fracture face, where secondary IG cracks were present in the specimen surface region. The slice of approximately 100 μm was electropolished in a solution of 5% perchloric acid in butoxyethanol, using a Tenupol-2 polishing unit operating at approximately 20 °C and a voltage of 30 V DC. The perforated slice was examined with a 300 kV Jeol 3010 transmission electron microscope.

3. Results

3.1. SSRT tests

In this work, we selected three different parameters; the strain to IG crack initiation, the number of IG cracking zones and the IG cracking ratio to quantify the SSRT test results. The strain to IG crack initiation was estimated from the stress–strain curves. Typical curves during the SSRT tests in inert gas as well as in oxygenated water are shown in Fig. 2, at different neutron fluences and the unirradiated condition. The curve in water deviates from the one in inert gas when both curves are superposed. It is seen that the strain to fracture in oxygenated water is smaller than that in inert gas, due to occurrences of non-ductile fracture. The strain to the deviating point was assumed to be the strain to which non-ductile cracks initiate during the SSRT tests in oxygenated water. Since all the specimens tested in oxygenated water were more or less of IG cracking mode on the periphery of the fracture surface by SEM observations, the non-ductile cracks were virtually identical to IG cracks. Thus we define the strain to IG crack initiation to be strain to the deviating point from an engineering viewpoint.

The number of IG cracking zones and the IG cracking ratio on the fracture surface were measured by the SEM fractographic examinations, even though the IG cracking ratio as a quantitative IASCC susceptibility indicator is erroneous and misleading [10].

3.1.1. Tensile behaviors in inert gas

Table 3 lists mechanical properties of the unirradiated and irradiated, thermally sensitized 304 SS in inert gas, which were determined from the stress–strain curves for various fluences. Fig. 3 shows tensile properties as a function of fluence. Yield and ultimate tensile stresses increase steadily with fluence (Fig. 3(a)), and uniform elongation decreases with fluence, except for at 1.1×10^{20} n/cm^2 where the value unsteadily changes (or slightly rises) (Fig. 3(b)). The irregular change in uniform elongation at this fluence seems to be due to a change in deformed microstructure. Thus TEM examination of deformed microstructures is required for identifying the cause of the irregular change at this fluence.

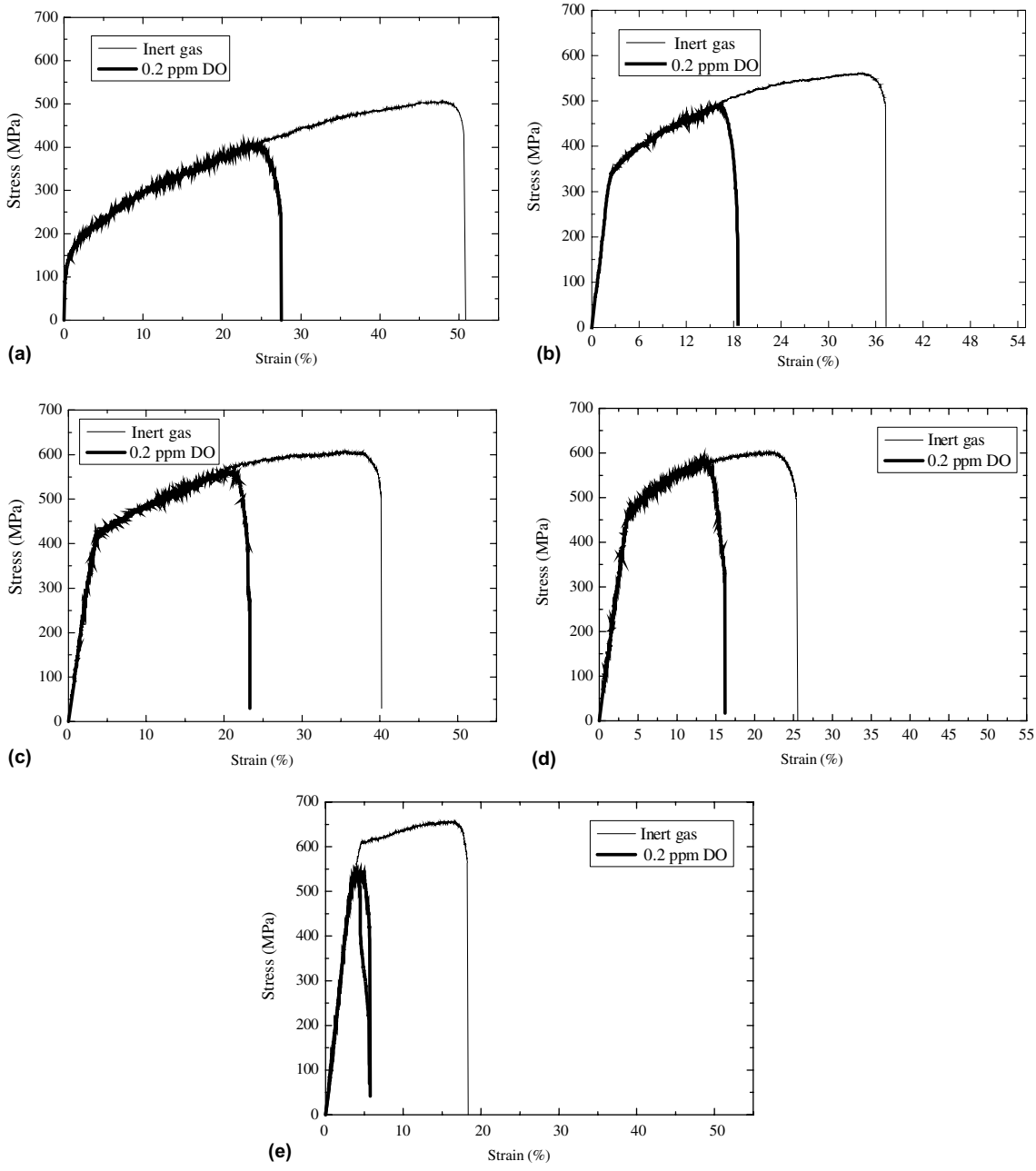

Fig. 2. Typical stress–strain curves of the thermally sensitized 304 SS during the SSRT tests in inert gas and in water containing 0.2 ppmDO at different neutron fluences: (a) unirradiated, (b) 7.5×10^{19} n/cm^2, (c) 1.1×10^{20} n/cm^2, (d) 6.2×10^{2} n/cm^2, and (e) 1.2×10^{21} n/cm^2.

SEM observations of fracture surface showed that the 1.2×10^{21} n/cm^2 specimen only revealed IG cracking among all the specimens tested in inert gas. The fracture surface in inert gas at 1.2×10^{21} n/cm^2 has totally 11 IG cracking zones on the periphery, resulting in the IG cracking ratio of 8%, as shown in Fig. 4.

3.1.2. IG cracking response in oxygenated water

Table 4 summarizes the strain to crack initiation, the number of IG cracking zones and the IG cracking ratio for all the specimens tested in oxygenated water. The strain to crack initiation is defined above. The number of IG cracking zones and the IG cracking ratio were esti-

Table 3
Mechanical properties of the unirradiated and irradiated, thermally sensitized 304 SS, tested by SSRT in inert gas

Fluence (n/cm^2)	Tensile stress (MPa)		Elongation (%)		Fracture mode
	Yield stress	Ultimate stress	Uniform	Non-uniform	
Unirrad.	144	504	48	3	Ductile
7.5×10^{19}	344	562	34	3	Ductile
1.1×10^{20}	406	608	36	4	Ductile
6.2×10^{20}	463	602	22	3	Ductile
1.2×10^{21}	608	656	16	2	IG fracture (8%)

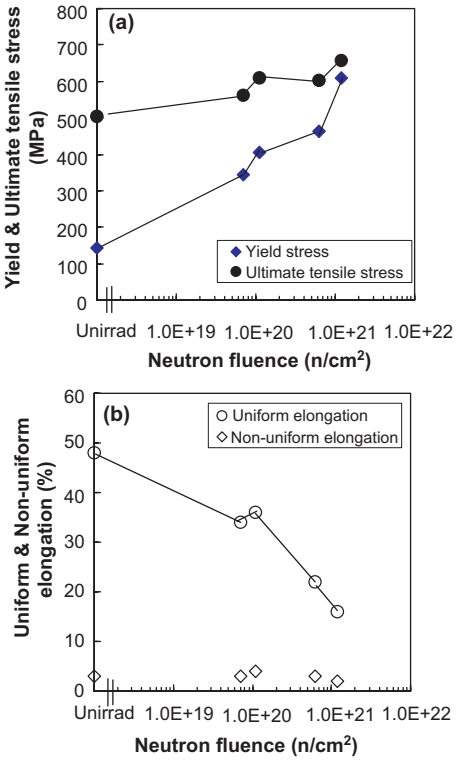

Fig. 3. Tensile properties as a function of fluence for the unirradiated and irradiated, thermally sensitized 304 SS: (a) yield and ultimate tensile stresses, and (b) uniform and non-uniform elongations.

mated from the SEM examination of fracture surface. Examples of fracture surface in oxygenated water are shown in Fig. 5 at 1.2×10^{21} and 1.1×10^{20} n/cm^2, and the unirradiated condition. The 1.2×10^{21} n/cm^2 specimen has IG cracking of 33%, consisting of 6 IG cracking zones (Fig. 5(a)) extending deeper than those in inert gas. With neutron fluence lowering, the IG cracking ratio and the number of IG cracking zones on the fracture surface reduced to 1% and only one IG cracking zone, respectively, for 1.1×10^{20} n/cm^2 (Fig. 5(b)) and then again they increased to 10% and four zones, respectively, for the unirradiated condition (Fig. 5(c)).

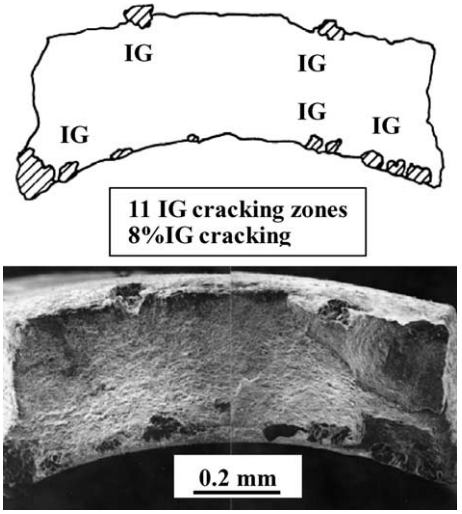

Fig. 4. Fracture surface of the thermally sensitized 304 SS irradiated to 1.2×10^{21} n/cm^2 and tested by SSRT in inert gas. IG cracking zones are present on the periphery.

Table 4
Summary of the strain to IG crack initiation, the number of IG cracking zones, and the IG cracking ratio for all the specimens tested by SSRT in oxygenated water

Fluence (n/cm^2)	The strain to IG crack initiation (%)	The number of IG cracking zones	The ratio of IG cracking (%)
Unirrad.	24	2	12
Unirrad.	22	4	10
7.5×10^{19}	12.5	3	16
1.1×10^{20}	15.5	1	4
1.1×10^{20}	23	2	1
6.2×10^{20}	9.5	2	7
1.16×10^{21}	0.5	3	31
1.22×10^{21}	0	6	33

Fig. 6 shows strain to IG crack initiation in water, along with uniform elongation in inert gas, as a function of neutron fluence. The strain to IG crack initiation decreases steadily with fluence of up to 7.5×10^{19} n/cm^2

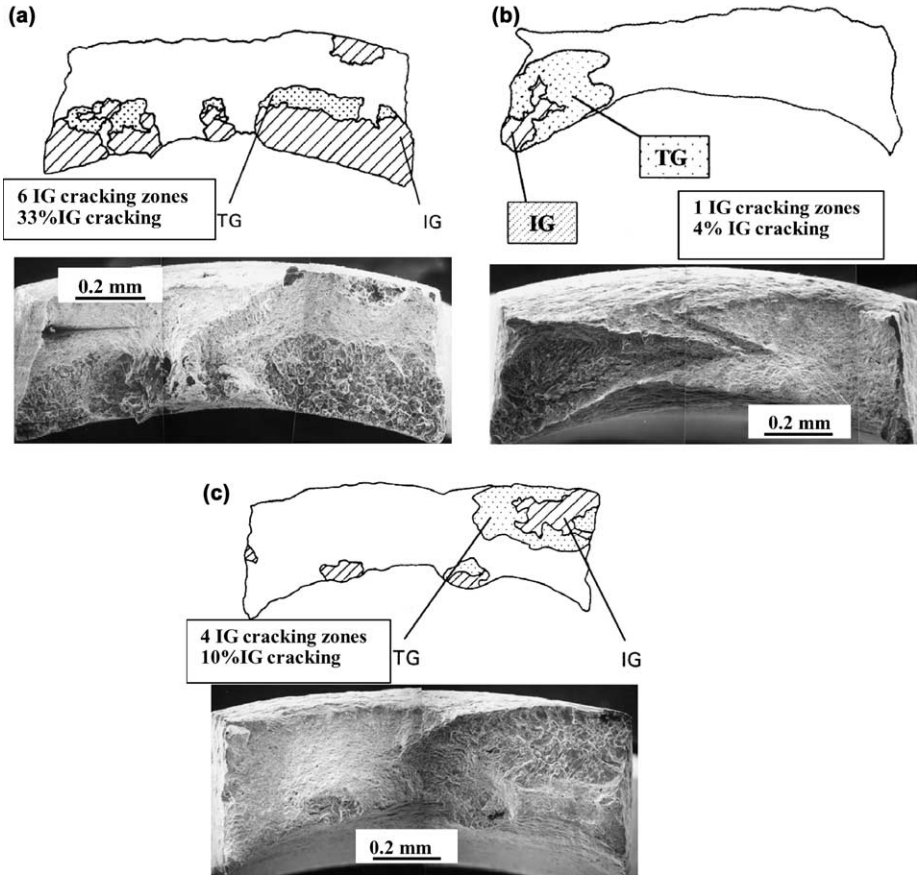

Fig. 5. Fracture surface of the thermally sensitized 304 SS irradiated to different neutron fluences and tested by SSRT in oxygenated water: (a) 1.2×10^{21} n/cm^2, (b) 1.1×10^{2} n/cm^2 and (c) unirradiated condition.

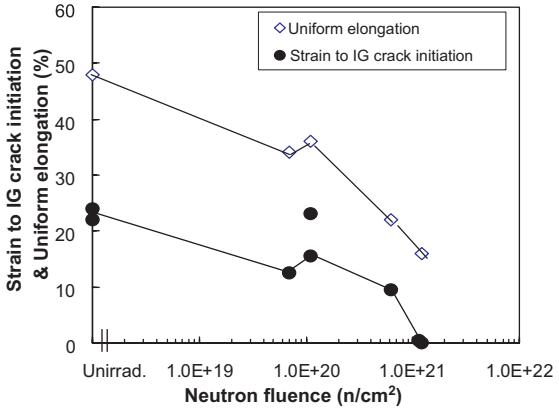

Fig. 6. Strain to IG crack initiation as a function of neutron fluence for the unirradiated and irradiated, thermally sensitized 304 SS tested by SSRT in oxygenated water, along with uniform elongation in inert gas.

with a slight rise at 1.1×10^{20} n/cm^2, followed by rapid reduction above this fluence. It is found that the change in strain to IG crack initiation with fluence is analogous to that for the uniform elongation and that the anomalous rise in IG crack initiation strain at 1.1×10^{20} n/cm^2 is also similar to each other, although the IG crack initiation strain is smaller than uniform elongation due to non-ductile failure of the material in oxygenated water. However the difference between uniform elongation and the IG crack initiation strain became smaller with fluence above 1.1×10^{20} n/cm^2 in particular, indicating that the initiation of IG cracks becomes earlier with fluence above 1.1×10^{20} n/cm^2.

Fig. 7 shows a plot of the IG cracking ratio and the number of IG cracking zones in water as a function of neutron fluence. The IG cracking ratio of 10–15% at the unirradiated condition and a lower fluence of 7.5×10^{19} n/cm^2 reduced down to only a few % at 1.1×10^{20} n/cm^2 and then increased with fluence, particularly at 1.2×10^{21} n/cm^2. The change in the number of IG cracking zones with fluence is also similar to that for the IG cracking ratio despite of only a small number of the specimens examined. Apparently the irradiated, thermally sensitized material revealed an anomalous IG

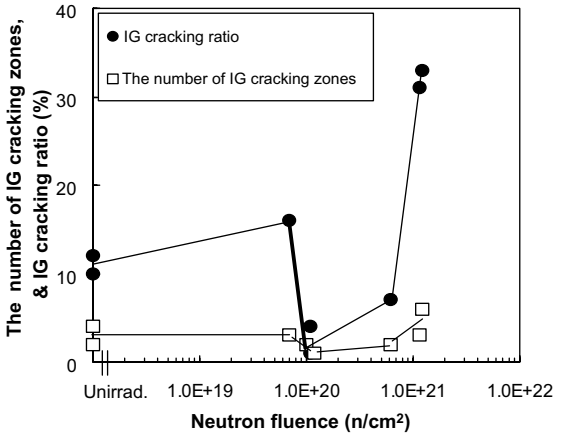

Fig. 7. The IG cracking ratio and the number of IG cracking zones as a function of neutron fluence for the unirradiated and irradiated, thermally sensitized 304 SS tested by SSRT in oxygenated water.

cracking responses represented with IG cracking ratio as a function of fluence, and that this trend of IG cracking ratio is consistent with that for the number of IG cracking zones. This implies that the anomalous change in % IG cracking with fluence originated from that for the number of IG cracking sites in water. However the trend of IG cracking response is quite different from the one for strain to IG crack initiation as shown in Fig. 6. Thus the fluence dependent change in IG cracking ratio is not brought about by an earlier onset of IG cracking but by the fluence dependent change in the number of IG crack initiation sites. It is also noticeable that a border fluence is present, discriminating the IG cracking response between above and below 1.1×10^{20} n/cm^2. The presence of the border fluence of around 1×10^{20} n/cm^2 is common to the three parameters – the uniform elongation, the strain to IG crack initiation and the IG cracking ratio as a function of neutron fluence.

3.2. Detailed fractographic examinations

3.2.1. Fracture surface

The 1.2×10^{21} n/cm^2 specimen revealed IG fracture in inert gas. Typical IG facet patterns of the fracture surface at the near surface region of the specimen are shown in Fig. 8. The rough and smooth patterns are presented, corresponding to carbides precipitated and carbides free grain boundaries and/or annealing twin boundaries (Fig. 8(a)), indicating that the IG facets were generated in the early stage of plastic deformation. Some of the rough facet patterns indicate clear and dense deformation step markings running in parallel with each other in the interior of the IG cracks (Fig. 8(b)). The planar steps must

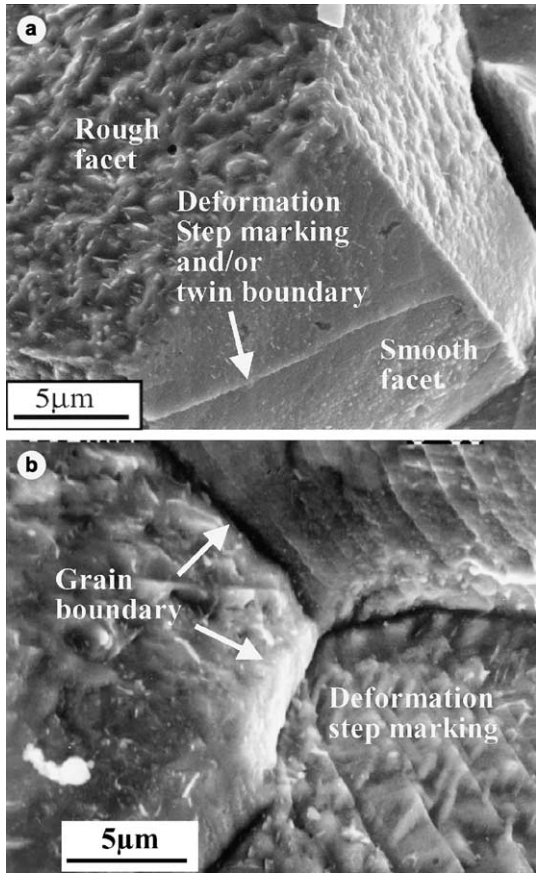

Fig. 8. Typical IG facet patterns of the fracture surface in inert gas for the thermally sensitized 304 SS irradiated to 1.2×10^{21} n/cm^2: (a) rough and smooth facet pattern at the near surface region, and (b) deformation step marking on an IG facet away from the surface region.

have been induced by plastic deformation localization during the SSRT in inert gas. The characteristic deformation step marking on the IG facets is an important evidence for the mechanically induced IG cracking. More detailed morphologies have been presented elsewhere [8].

A typical IG facet of the 1.2×10^{21} n/cm^2 specimen generated in oxygenated water is shown in Fig. 9. The IG facet is covered with oxides or corrosion product deposition on the fracture surface (Fig. 9(a)). A careful examination indicates that some of the IG facet surface have deformation step marking under the corrosion product deposition (Fig. 9(b)). It is interesting to note that the deformation step marking identified beneath the corrosion product deposition is likely to be caused by plastic deformation localization during the SSRT tests. Thus the IG cracking may have occurred in the mechanically induced process in the same manner as that in inert gas (Fig. 8(b)).

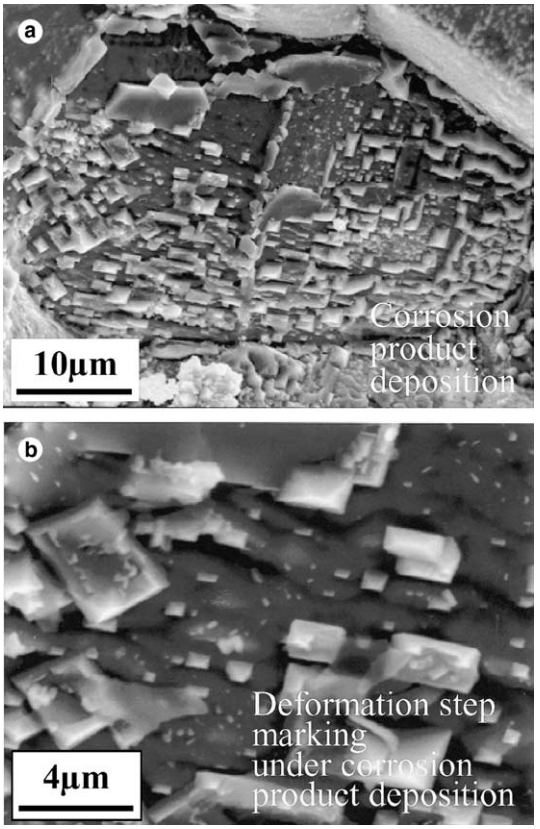

Fig. 9. A typical IG facet in oxygenated water for the thermally sensitized 304 SS irradiated to 1.2×10^{21} n/cm^2; (a) IG facet covered with corrosion product deposition and (b) deformation step marking under corrosion product deposition.

3.2.2. Specimen surface

Surface appearances of the 1.2×10^{21} n/cm^2 specimen fractured intergranularly in inert gas were shown in Fig. 10. It is seen that numerous small IG cracks are present on the concave surface and on the side surface as well, which are linked to localized plastic deformation bans (Fig. 10(a)). It is also found that a few large IG cracks in nature are present, which are linked to possible localized deformation bands lying at 45° to the gauge length on the convex surface (Fig. 10(b)), although the presence of the thick oxide layer on the specimen surface prevented a detailed examination of these features. The IG cracking sites and the deformation banding are apparently linked together to each other.

The specimen surface of the samples tested in water containing 0.2 ppmDO was heavily contaminated with corrosion product deposition, which prevented from identifying characteristic of detailed fractographic features. Nevertheless careful examinations before and after removal of oxide and corrosion product deposition showed important evidences of mechanically induced cracking in water environment. Fig. 11 represents surface appearances of the 1.2×10^{21} n/cm^2 material intergranularly fractured in water. The concave surface appearance showed a few secondary cracks before removal of the oxide layer (Fig. 11(a)). After removal of the oxide films more cracks are identified on the concave surface (Fig. 11(b)), and the linkage of the secondary cracks and plastic deformation localization is observed more clearly on the side surface after removal of the oxide layer (Fig. 11(c)).

Specimen surface observation was also made for the two 1.1×10^{20} n/cm^2 samples that have IG cracking ratios of only a few % in oxygenated water. One of the two specimen had only 1% IG cracking (a grain) on fracture surface without any apparent IG cracks on the specimen surface region. After removal of the corrosion product deposition and oxide film, however, two small IG cracks were detected on the concave surface, as exhibited in Fig. 12. The IG cracks resemble those generated on the specimen surface of the 1.2×10^{21} n/cm^2 specimen in inert gas as indicated in Fig. 10(b), in such way that the IG cracks along the grain boundary are closely connected to localized plastic deformation bands. This proves that the process of radiation induced plastic deformation localization is a primary factor for causing IG cracking in oxygenated water for the 304 SS specimens irradiated to fluences of more than 1.1×10^{20} n/cm^2.

At the lower fluences below 1.1×10^{20} n/cm^2, where plastic deformation localization is not discernible by SEM observation, it is still uncertain what process is applicable for the IG crack initiation process. However, the unirradiated 304 SS sample fractured in mixed modes of IG and TG cracking in oxygenated water. Surface appearance is found to be heavily deformed and a secondary crack of TG cracking mode in addition to IG cracking appears to be induced by a homogeneous deformation process but not by a corrosion process, as shown in Fig. 13.

3.3. Microstructural examinations

Comprehensive TEM microstructures of the thermally sensitized 304 SSs irradiated to different fluences and deformed to fracture in inert gas were examined, and their results were summarized in Table 5.

Typical deformation microstructures were presented in Fig. 14 at the unirradiated condition, and at fluences of 7.5×10^{19}, 1.1×10^{20} and 1.2×10^{21} n/cm^2. At the unirradiated condition, the dislocation cellular structures are predominant. The cell boundaries consisted of a random array of dislocations with very few dislocations present in the cell interiors, and also with presence of occasional planar defects, typically microtwins (Fig. 14(a)). At 7.5×10^{19} n/cm^2, deformation occurred by dislocation generation, movement and interaction, forming a cellular line. Dislocation structures formed are seen,

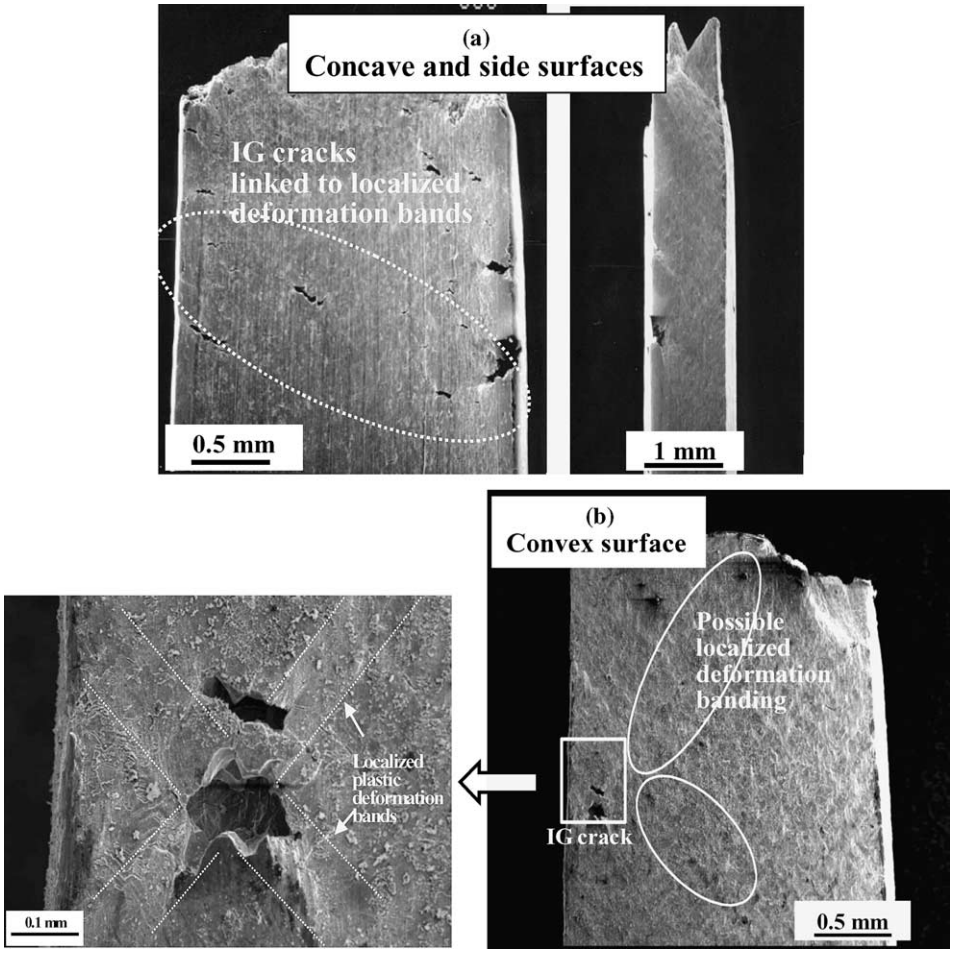

Fig. 10. Surface appearances of the 1.2×10^{21} n/cm^2 thermally sensitized 304 SS specimen fractured intergranularly in inert gas: (a) concave and side surfaces, and (b) convex surface.

with limited linear features/deformation twinning (upper right in the figure of Fig. 14(b)). Dislocation loops produced by irradiation were not obvious in the microstructure, although yield stress increased at this fluence. Radiation induced defects invisible may have brought about a significant hardening effect, leading to a tendency for the material to deform by twinning rather than dislocation generation and movement at least at low strains. In some regions a cellular line dislocation structure is seen to be forming.

At 1.1×10^{20} n/cm^2, the general deformation microstructure is primarily of dislocations forming a cellular structure. In some regions the cellular network was well developed. Radiation induced dislocation loops were not readily observed. Within the dislocation structure a population of linear features/deformation twins can be observed, lying on the fcc [1 1 1] type planes (Fig. 14(c)). At 1.2×10^{21} n/cm^2, microstructures are dominated by large numbers of linear features/deformation twins present on all variants of the [1 1 1] type planes (Fig. 14(d)). The number and spacing of deformation twins varied from region to region, depending on the grain orientation. A high number density of radiation induced dislocation loops is present away from deformation twins and grain boundaries. There were no regions containing line dislocation, even at high magnification examination.

Fig. 15 shows typical deformation microstructures in the surface region at unirradiated condition and 1.2×10^{21} n/cm^2. The unirradiated deformation microstructures also consist of dislocation cell structures in grain matrices, and carbide precipitates at the grain boundary (Fig. 15(a)). In addition to grain boundaries, annealing twin boundaries are occasionally observed free of carbide precipitation. Since the annealing twin boundaries are formed during re-crystallization heat treatment processes, they are common features in unirradiated and irradiated materials. The deformation

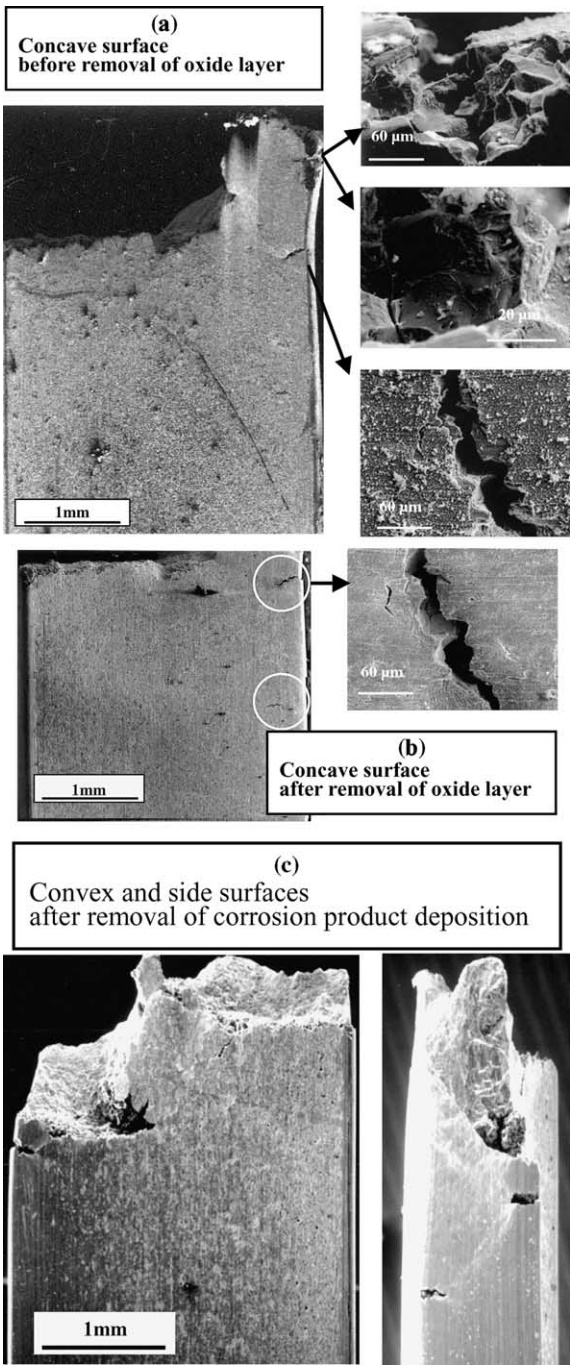

Fig. 11. Surface appearances of the 1.2×10^{21} n/cm^2 thermally sensitized 304 SS specimen intergranularly fractured in oxygenated water: (a) concave surface before removal of oxide layer, (b) concave surface after removal of oxide layer, and (c) convex and side surfaces after removal of corrosion product deposition.

microstructures at 1.2×10^{21} n/cm^2 are characteristic of linear features and microtwins in grain matrices, and carbide precipitates at the grain boundary (Fig. 15(b)). The selected area diffraction pattern identified the linear features to consist of deformation twins and not of dislocation lines in the channel shaped pattern, although such inhomogeneous deformation microstructures in irradiated materials are generally termed as dislocation channel. The microtwins in the grain matrices are emitted from the grain boundary and the carbide precipitates at the grain boundary. The high density of microtwins is an important evidence for high stress and strain concentration at the grain boundary. More detailed TEM examination results have been presented separately [8].

4. Discussion

The results of the SSRT test in oxygenated water on the thermally sensitized 304 SSs have shown that the IG crack initiation behaviors as a function of neutron fluence change at a boarder fluence of around 1×10^{20} n/cm^2. Neutron fluence dependent uniform elongation and ultimate tensile stress also irregularly changes at the same fluence. SEM examinations have shown that IG crack initiation sites tend to link to localized plastic deformation bands. Typical TEM deformation microstructures at around the boarder fluence are in the transition from homogeneous dislocation microstructure to inhomogeneous deformation microstructure. Apparently these results suggest that the boarder fluence has specific meanings related to mechanism of IG crack initiation in the irradiated, thermally sensitized 304 SSs under environment of oxygenated water. The anomalous IG cracking responses at the boarder fluence are unable to interpret in terms of the grain boundary Cr depletion theory at all, due to the fact that IG cracking occurrences reduced extremely at this fluence, as seen in Fig. 7, without regard to further Cr depletion predictable due to RIS at grain boundaries. The neutron fluence dependent IG crack initiation behaviors of the materials deformed and fractured in oxygenated water are obviously associated with fractographic and microstructural features examined. Thus we have to comprehensively discuss the results of the SSRT tests, SEM fractographic morphologies and TEM deformed microstructures, to find the actual meanings of the border fluence and to identify mechanism of irradiation assisted stress corrosion crack initiation for the thermally sensitized 304 SSs.

The strain to IG crack initiation, the IG cracking ratio and the number of IG crack initiation sites in oxygenated water as a function of neutron fluence are distinguished between above and below the border fluence of around 1×10^{20} n/cm^2, as demonstrated in Figs. 6 and 7. The presence of the border fluence is also seen in neutron fluence dependent uniform elongation that is determined by the SSRT in inert gas environment, as shown in Fig. 3. Similarly, the irradiated thermally trea-

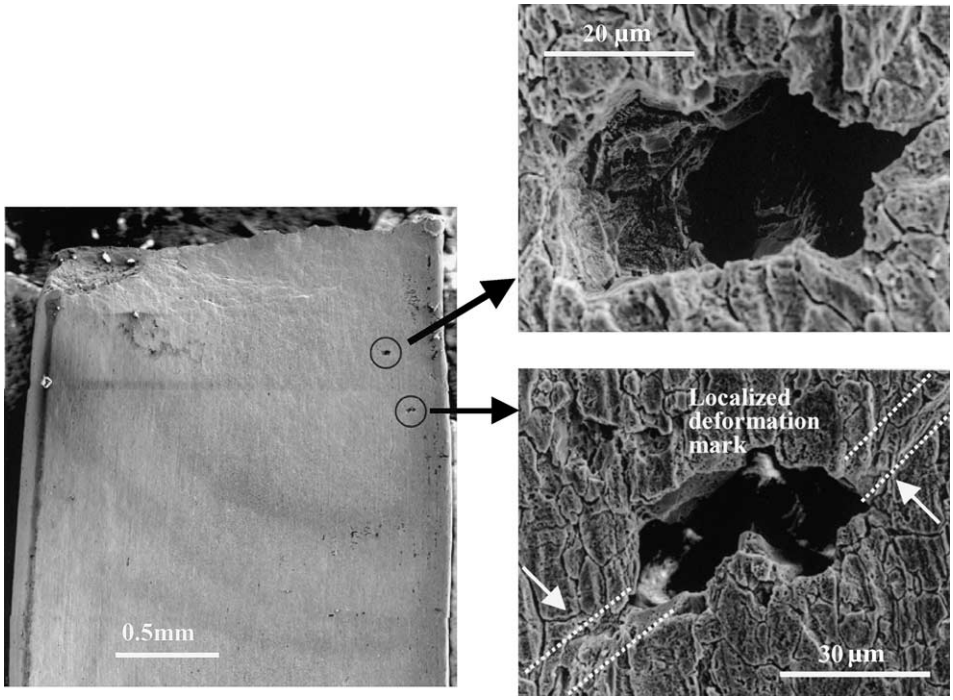

Fig. 12. Surface appearances of the 1.1×10^{21} n/cm^2 thermally sensitized 304 SS specimen intergranularly fractured in oxygenated water (after removal of the oxide layer).

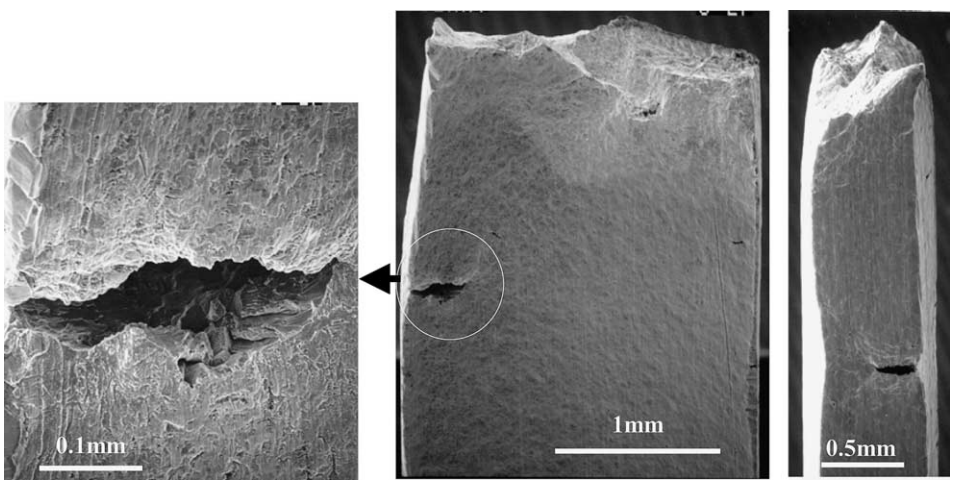

Fig. 13. Surface appearances of the unirradiated thermally sensitized 304 SS specimen intergranularly and transgranularly fractured in oxygenated water (after removal of the oxide layer).

ted 304LSSs that were tested by the SSRT in water containing 8 ppmDO, together with the thermally sensitized 304 SSs in this work, have an occurrence of IG cracking at the border fluence of around 1×10^{20} n/cm^2 [11], above which the IG cracking ratio characteristically rises. This indicates that the 304LSS has phenomenologically an IASCC threshold fluence of around 1×10^{20} n/cm^2, and that the border fluence for the thermally sensitized 304 SS and the IASCC threshold fluence for the thermal treated 304LSS are identical to each other. Since the two materials were irradiated at the same time in the same irradiation capsules and reactor, and tested by the SSRT at the same conditions in the same test facilities, the border fluence and the IASCC threshold fluence

Table 5
Summary of TEM deformed microstructures for the unirradiated and irradiated, thermally sensitized 304 SS

Fluence (n/cm^2)	Deformation level (distance from fracture face)	Radiation induced dislocation loops	Other dislocation forms	Planar defects (or Microtwins)	Linear feature/deformation twins
Unirrad.	Undeformed	No	Low number density	No	No
	Low (12 mm)	No	Primary slip and start of cellular formation	Large number of defects in grain interior and boundary regions	No
	Medium	No	Increased interaction forming sub-structure of cells	Reduction in number density	No
	High (1 mm)	No	Complete cellular structure with refined cell walls	Only occasionally observed	No
7.5×10^{19}	Medium	Not readily observed	Start of cellular formation	Large number of defects in grain interior and boundary regions	Yes, simple mode
1.1×10^{20}	Low	–	–	–	–
	Medium (8 mm)	Not readily observed; small loop, low number density	Dislocations on primary slip planes and initial cellular formation	Small nuclei only	Limited deformation twins in partial regions
	High (1.3 mm)	The same	Dislocations on primary slip planes and advanced cellular formation	The same	Limited deformation twins
1.2×10^{21}	Un deformed	Loop size = 6.3 nm, number density = 3.1×10 m	No line dislocation	No	No
	Low (12 mm)	The same	The same	No	Yes
	Medium	The same	The same	Small number of nuclei in grain interior and boundary regions	Deformation twinning on all [1 1 1] plane variants
	High (1 mm)	The same	The same	Small number of nuclei in grain interior and boundary regions	Frequency of twins increased

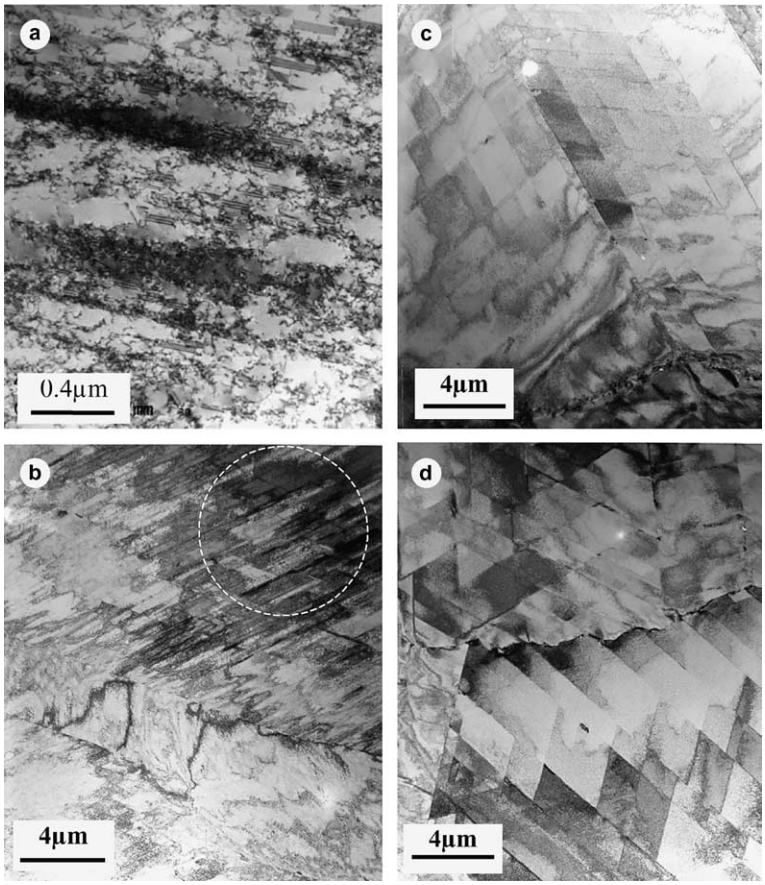

Fig. 14. Typical deformation microstructures of the thermally sensitized 304 SS irradiated to different neutron fluences and tested by SSRT in inert gas: (a) unirradiated, (b) 7.5×10^{19} n/cm^2, (c) 1.1×10^{20} n/cm^2, and (d) 1.2×10^{21} n/cm^2.

for the two materials may have a common mechanistic basis at around 1×10^{20} n/cm^2, though no specific role of sensitized microstructures on the IG crack initiation of the thermally sensitized material is confirmed by detailed fractographic and microstructural examinations yet.

The TEM deformation microstructures at the border fluence are in the transition from dislocation structures to deformation twinning structures, although radiation induced dislocation loops are not readily observed yet, as noted in Table 5. This implies that radiation induced defects, even invisible yet, contributing to radiation hardening are significantly important for the evolutions of inhomogeneous deformation twinning. At 1.2×10^{21} n/cm^2, the deformation microstructures were typical of linear features/deformation twinning, with radiation induced dislocation loops visible with a size of 6.3 nm and a density of 3.1×10^{22} m^{-1} as shown in Table 5. This characterization of radiation damage defects is consistent with the literature data [6] regardless of the thermally, sensitized material. Although degradation of mechanical properties in irradiated materials, typically reduction in uniform elongation, is primarily ascribable macroscopically to radiation induced localized plastic deformation bands and microscopically to dislocation channeling [12] in general, the TEM deformation microstructures of the irradiated, thermally sensitized 304 SS were not characteristic of dislocation channeling in this work. Alternatively the presence of deformation twins without dislocation lines, named linear features/deformation twinning, in the irradiated deformation microstructures was confirmed by the selected area diffraction analyses [8]. Thus the predominant deformation microstructures above the border fluence were of linear features/deformation twins, whereas those below the boarder fluence and at the unirradiated condition were of prevailing homogeneous dislocation structures, as shown in Fig. 14.

The IG crack initiation sites tended to link to localized plastic deformation bands on the surface of the fractured, thermally sensitized 304 SS specimen in oxygenated water. The linkage of IG crack initiation sites

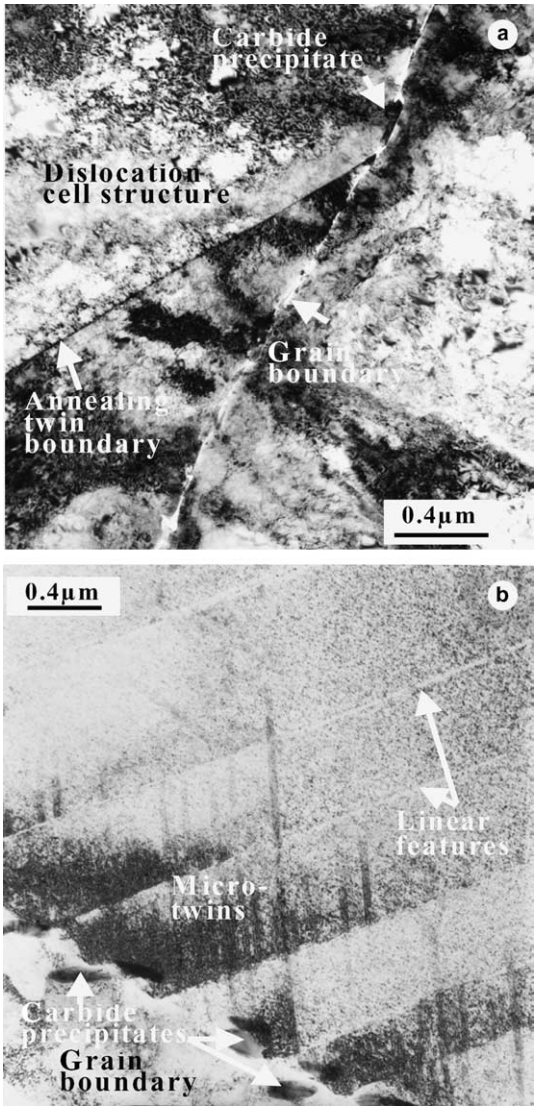

Fig. 15. Typical deformation microstructures in the surface region of the thermally sensitized 304 SS tested by SSRT in inert gas: (a) unirradiated condition, and (b) 1.2×10^{21} n/cm^2.

to localized plastic deformation bands was further verified at earlier stages of deformation by the interrupted SSRT tests in oxygenated water. Fig. 16 shows an example of IG crack initiation site on the 6.2×10^{20} n/cm^2 sample strained up to about 4% in water containing 0.2 ppmDO [13]. It is seen that some small IG cavities on the specimen surface are linked to a localized plastic deformation band (Fig. 16(a)), and some are surrounded with slightly deformed matrix even though the linkage to the deformation localization is unclear yet (Fig. 16(b)). It should be noted that all of the sites for IG crack initiation do not readily grow, even though numerous small IG cracks are formed in the early stage of deformation, but only few IG cracks initiated may be able to grow to fracture in the lower DO water. Therefore the IG crack initiation of the irradiated, thermally sensitized 304 SS in oxygenated water above the border fluence is caused by radiation induced deformation twins interacted with grain boundaries in the same way as the IG crack initiation in inert gas for the 1.2×10^{21} n/cm^2 specimen. In another words, radiation induced changes in plastic deformation microstructures from homogeneous dislocation structures to inhomogeneous deformation twinnings are the mechanistic basis of the border fluence, and neither radiation induced dislocation loops visible nor radiation induced chromium depletion at grain boundaries are.

The border fluence of around 1×10^{20} n/cm^2 discriminates the IG cracking process specific to the irradiated material from the conventional IGSCC process, although IG cracking in oxygenated water occurred at all the fluences tested and the unirradiated condition. In the IG cracking process above the border fluence, the IG cracking ratio increased rapidly with increasing fluence. Correspondingly onsets of localized deformation became earlier, resulting in an increase in the number of macroscopic localized deformation bands and/or in the population density of microscopic deformation twins with increasing fluence. This may lead to an increase in the number of IG crack initiation sites in oxygenated water, because the deformation twins act as the source of high stress concentration at the interaction with grain boundaries [14]. In the IGSCC process below the border fluence, the thermally sensitized 304 SSs unirradiated and irradiated to the lower fluences deform primarily by dislocation generation and movement as described in Table 4. Nevertheless the concept of local stress and strain concentrations at the grain boundaries may be probable as well as in the case of above the border fluence. The most conspicuous and detrimental features at grain boundaries may be the presence of Cr carbides precipitate as a source of stress and strain concentration. The grain boundary carbides precipitation is shown in Fig. 17 for the 7.5×10^{19} n/cm^2 thermally sensitized 304 SS deformed to fracture. Apparently microtwins in the near-grain boundary regions running up to carbide precipitates, indicate that carbide precipitates at grain boundaries are associated to the early stage of deformation twinning. The grain boundary carbide precipitates may behave similarly in the unirradiated thermally sensitized 304 SS as well. A general observation of deformation microstructures for the unirradiated material is that structure, distribution and density of both dislocations and planar defects (stacking faults or microtwins) vary depending on deformation level and at high deformation level, complete cellular structures evolve with refined cell walls, with only occasional microtwins. More TEM examinations of deformation microstructure are required to determine the

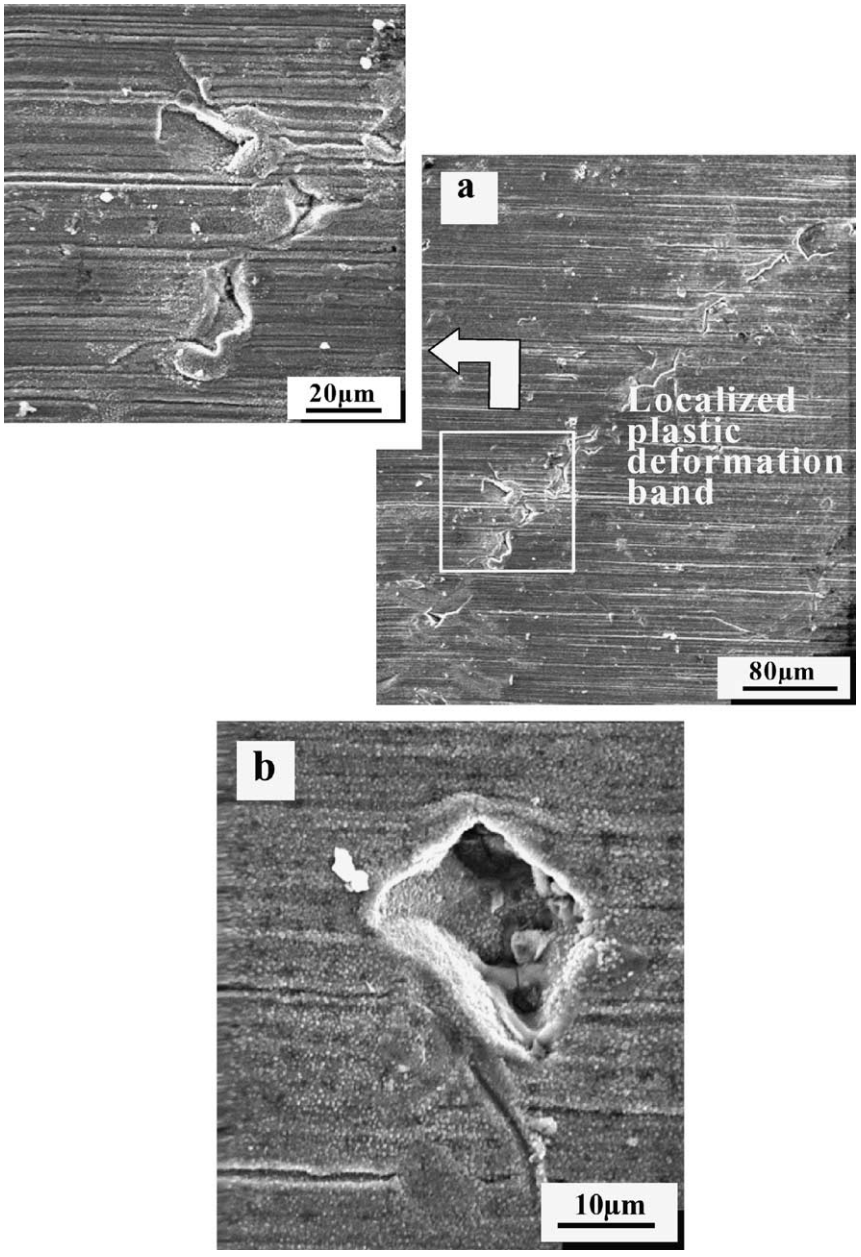

Fig. 16. An example of IG crack initiation site at a strain of about 4% on the surface of the 6.2×10^2 n/cm^2 thermally sensitized 304 SS. The specimen was tested by the interrupted SSRT in oxygenated water: (a) a localized plastic deformation band with IG crack nucleation and initiation, and (b) a small IG cavity with surrounding edges and matrix deformed slightly.

role of carbide precipitates on the IGSCC initiation process. Therefore we conclude that the specific IG cracking above the border fluence indicates IASCC and the border fluence is equivalent to an IASCC threshold fluence for the irradiated, thermally, sensitized 304 SS, despite the fact that the terminology of IASCC is originally given to the non-sensitized austenitic steels without microstructural definition.

The IASCC threshold fluence of around 1×10^{20} n/cm^2 for the thermally sensitized 304 SS in this work is apparently lower than the IASCC threshold fluence of about 5×10^{20} n/cm^2 that has been admitted for the solution annealed 304 SS. This is not due to sensitized microstructures characteristic of the thermally sensitized material, since the IASCC threshold fluence for the thermally sensitized 304 SS is identical to that for the

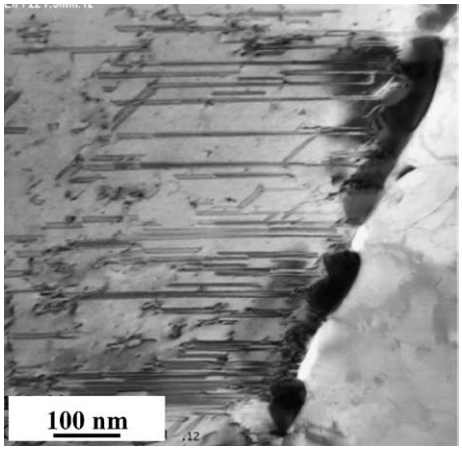

Fig. 17. Grain boundary carbides precipitate in the 7.5×10^{19} n/cm^2 thermally sensitized 304 SS tested by SSRT in inert gas. Microtwins are running up to carbides precipitate in the near grain boundary region.

304LSS as discussed previously. Alternatively it is noted that the lower IASCC threshold fluence was determined for the test reactor irradiated materials and for the tests in the 0.2 ppmDO water environment in this work, in comparison to that for the BWR irradiated materials and for the tests in the 32 ppmDO water environment in the literature. Such a water environment as low as 0.2 ppmDO may not be attributable to the lower IASCC fluence, as will be discussed later. Resolution is needed why and how the test reactor irradiation conditions affected the lower IASCC threshold fluence value. In the present work, neutron irradiation was made in the JMTR up to 1.1×10^{20} n/cm^2 at higher neutron fluxes and at lower irradiation temperatures than in the BWR, as seen in Table 2. The neutron fluxes of the order of 10^{13} n/cm^2 in the JMTR were one to two orders of magnitude larger than those in the BWR. Although data available for evaluating neutron flux effect are few, we can estimate the neutron flux effect on the IASCC threshold fluence, based on mechanical properties changes with neutron flux for type 304 SSs irradiated in the BWR. It has been recognized that yield stress increases with increasing neutron flux at fluxes of 5×10^{12}–1×10^{13} n/cm^2/s in the fluence range of the order of 10^{20} n/cm^2 [15]. Such neutron flux effect on mechanical properties may be brought about by the larger radiation damage rate and higher damage defects accumulated. The higher neutron fluxes in the JMTR may tend to produce more damage defects accumulated even in the same fluence level, resulting in lowering the IASCC threshold fluence. Moreover, the lower irradiation temperatures in this work by about 100 °C would have affected IASCC fluence threshold for the materials more considerably than we expected. This is because diffusivity of damage defects and thermal stability of defect clusters tend to become lower at the lower irradiation temperature than at the higher temperature, resulting in retarding recombination of vacancies and interstitials produced by neutron irradiation, in general. In this way the higher neutron flux and lower irradiation temperature in the JMTR irradiation should have been effective for producing more damage defects than the lower flux and higher temperature in BWR. Thus the irradiation conditions, especially irradiation temperature, in the JMTR may have brought about the lower IASCC threshold fluence for the material. Therefore the lower IASCC threshold fluence for the thermally sensitized 304 SS should be ascribable to the lower irradiation temperature and higher neutron flux in the test reactor irradiation. This means that the IASCC threshold fluence for the thermally sensitized material would be consistent with that for the solution annealed one, if the same irradiation conditions were applied for the two materials.

Concerning the DO dependence on the IASCC susceptibility, it has been believed that the IASCC susceptibility decreases and the IASCC threshold fluence increases with decreasing DO. These opinions have been established from the results of the SSRT tests on the solution annealed austenitic stainless steels irradiated in BWR, based on the RIS induced chromium depletion theory. For example, Kodama et al. [16,17] reported that IASCC susceptibility increased markedly for fluences exceeding 10^{21} n/cm^2 at 32 ppmDO, and low DO water could effectively mitigate IASCC in relatively high fluence regions and that radiation induced chromium depletion may have been one of the dominant factors affecting IASCC resistance. Nowadays, however, it is quite erroneous to interpret their data in the manner that the reduction in %IGSCC with decreasing DO is brought about by preventing and/or retarding IG crack initiation. Attention should be paid to both contributions of IG crack initiation and growth processes to %IGSCC as an IASCC susceptibility indicator, when interpreting data of the fluence and DO dependent %IGSCC. According to the current understanding of SCC susceptibility, as a matter of fact, crack growth rate measurements are considered to be the most reproducible and statistically significant [18], and SCC crack growth rates are strongly influenced by water quality in addition to other factors [19]. When the SSRT tests are conducted at higher DO concentrations, IG cracking sites are usually connected to each other by larger crack growth rates. Based on the mechanism of IASCC initiation investigated in the present work, the IG crack initiation is caused by stress and strain concentrations at the grain boundaries interacted with radiation induced deformation twins, and the increase in %IGSCC with increasing neutron fluence is brought about by the increase in the number of IG crack initiation sites. The current knowledge of IASCC crack initiation and growth rate is useful to re-interpret the above data of Kodama et al., in that the larger %IGSCC

for fluences exceeding 10^{21} n/cm^2 at 32 ppmDO may probably be due to either large IG crack growth rates, IG crack initiation sites connected, or both. Kodama et al. also insisted effective mitigation of IASCC in relatively high fluence regions at lower DO, while we re-interpret their data in terms of relatively smaller number of IG crack initiation sites and a lower IG crack growth rate. Therefore it is concluded that the IASCC threshold fluence will remain unchanged with DO because the IG crack initiation is caused by the deformation localization, though IASCC susceptibility appears to increase with DO.

It should be kept in mind that the IASCC threshold fluence of about 5×10^{20} n/cm^2 for the BWR irradiated solution annealed 304 SSs was determined from the SSRT tests in 32 ppmDO water, without detailed fractographic and microstructural examinations. Such an extremely high DO water as 32 ppmDO may probably be injurious to search mechanistic traces, because the fracture surface and specimen surface are heavily contaminated with corrosion products deposition. Contaminated fracture surface and specimens surface enables us to prevent detailed SEM examinations. More importantly, IG cracks, once initiated, grow rapidly in higher DO water without leaving clear evidences for deformation markings on the IG facets. If the SSRT tests were performed in water containing higher DO in this work, no significant mechanical traces would be detected on the fracture surface and specimen surface. Thus the lower DO water environment is preferable to mechanistic investigation of IASCC initiation process.

5. Conclusions

(1) Neutron fluence dependent IG cracking behaviors of the thermally sensitized 304 SS in oxygenated water changed at a border fluence (around 1×10^{20} n/cm^2). Above the fluence deformation twinning specific to the irradiated material was predominant in the deformation microstructures, and localized deformation banding occurred earlier with increasing fluence. The crack initiation sites tended to link to the localized deformation bands. Thus the crack initiation was caused by the deformation bands interacted with grain boundaries.

(2) The border fluence discriminates the IG cracking process specific to the irradiated material from the conventional IGSCC process, though the IG cracking in oxygenated water occurred at all the fluences tested and the unirradiated condition. Thus the specific IG cracking indicates IASCC and the border fluence is equivalent to the IASCC threshold fluence for the irradiated, thermally sensitized 304 SS, despite the fact that the terminology of IASCC is originally given to the non-sensitized materials without microstructural definition.

(3) Above the IASCC threshold fluence, the number of IG cracking sites and the IG cracking ratio increased with increasing fluence in water containing as low as 0.2 ppmDO. This indicates that the increase in IASCC susceptibility with increasing fluence is due to the increase in the number of IG crack initiation sites. However, the IASCC threshold fluence will remain unchanged, though the IASCC susceptibility appears to increase, with increasing DO because the IG crack initiation is caused by the deformation localization.

(4) The IASCC threshold fluence for the thermally sensitized material was lower than the IASCC threshold fluence of about 5×10^{20} n/cm^2 admitted for the solution annealed one. This may be due to higher neutron fluxes and lower irradiation temperatures at the test reactor irradiation condition and not due to the sensitized microstructure, suggesting that the IASCC threshold fluence for the thermally sensitized material would be consistent with that for the solution annealed one, if the same irradiation conditions were applied for the two materials.

Acknowledgments

Authors are grateful to Ms T. Karlsen at IFE, Norway and Professor H. Matsui at Tohoku University, Japan for performing neutron irradiation of the materials at Halden Reactor and at JMTR, respectively. Thanks are also extended to Dr Cowan in BNFL, Berkeley, UK for performing the TEM works of the irradiated samples.

References

[1] For example, E. Forkhard, Welding Metallurgy of Stainless Steels, Springer-Verlag/Wien, 1988, p. 103.
[2] P.L. Andresen, F.P. Ford, S.M. Murphy, J.M. Perks, in: Proceedings of the Fourth International Symposium Environmental Degradation of Materials in Nuclear Power Systems – Water Reactors, NACE, 1990, p. 1.
[3] T.M. Angeliu, R. Horn, J. Walmsley, in: Proceedings of the Eighth International Symposium on Environmental Degradation of Materials in Nuclear Power Systems – Water Reactors, ANS, 1997, p. 649.
[4] J.T. Busby, G.S. Was, E.A. Kenik, J. Nucl. Mater. 320 (2002) 20.
[5] K. Fukuya, M. Nakano, K. Fujii, T. Torimaru, J. Nucl. Sci. Technol. 41 (2004) 594.
[6] S.M. Bruemmer, E.P. Simonen, P.M. Scott, P.L. Andresen, G.S. Was, J.L. Nelson, J. Nucl. Mater. 274 (1999) 299.
[7] T. Onchi, K. Hide, M.L. Castano, M. Navas, in: Proceedings of 10th International Conference on Environmental

Degradation of Materials in Nuclear Power Systems – Water Reactors, NACE, 2001.
[8] T. Onchi, K. Dohi, N. Soneda, J.R. Cowan, R.J. Scowen, M.L. Castano, J. Nucl. Mater. 320 (2003) 194.
[9] K. Hide, T. Onchi, M. Mayuzumi, in: Proceedings 10th International Conference on Environmental Degradation of Materials in Nuclear Power Systems – Water Reactors, NACE, 2001.
[10] T. Onchi, K. Hide, M. Mayuzumi, T. Hoshiya, Corrosion 56 (2000) 451.
[11] M. Navas, M.L Castaño, D. Gómez-Briceño, T. Onchi, in: Proceedings 11th International Conference on Environmental Degradation of Materials in Nuclear Power Systems – Water Reactors, ANS, 2003.
[12] M.S. Wechsler, The Inhomogeneity of Plastic Deformation, ASM, Ohio, 1973, p. 47.
[13] T. Onchi, M. Navas, M.L. Castano, unpublished work.
[14] K.S. Sree Harsha, Metal. Trans. 12A (1981) 365.
[15] T. Torimaru, M. Kodama, S. Tanaka, T. Nakamura, K. Asano, K. Kumagai, in: Proceedings at the 22nd Symposium on Effects of Radiation on Materials, 8–10 June 2004, Boston, USA, submitted for publication.
[16] M. Kodama, S. Nishimura, J. Morisawa, S. Suzuki, S. Shima, M. Yamamoto, in: Proceedings of the Fifth International Symposium on Environmental Degradation of Materials in Nuclear Power Systems – Water Reactors, ANS, 1991, p. 948.
[17] M. Kodama, R. Katsura, J. Morisawa, S. Nishimura, S. Suzuki, K. Asano, K. Fukuya, K. Nakata, in: Proceedings of the Sixth International Symposium on Environmental Degradation of Materials in Nuclear Power Systems – Water Reactors, TMS, 1993, p. 583.
[18] P.L. Andresen, in: Proceedings of the 10th International Conference on Environmental Degradation of Materials in Nuclear Power Systems – Water Reactors, NACE, 2001.
[19] P.L. Andresen, P.W. Emigh, M.M. Morra, R.M. Horn, in: Proceedings of the 11th International Conference on Environmental Degradation of Materials in Nuclear Power Systems – Water Reactors, NACE and TMS, 2003.